REVIEW ARTICLE | INSIGHT
https://doi.org/10.1038/s41567-022-01723-8

nature physics



# Imaging in complex media

Jacopo Bertolotti[1]✉ and Ori Katz[2]✉

**Imaging can take many forms—from optical microscopes and telescopes through ultrasonography to X-ray tomography. However, regardless of the imaging modality, the presence of a complex heterogeneous structure between the imaging system and the scene of interest limits the quality of the images that can be conventionally obtained. In this Review we outline recently introduced strategies to overcome the detrimental effects of scattering in optical imaging. In particular, we focus on approaches that either physically correct scattering using computer-controlled devices or employ computational inversion based on intrinsic correlations of light scattering. Despite focusing on optical techniques, this Review emphasizes the fundamental equivalence of the effects of scattering in different fields of imaging, using the scattering matrix formalism as a bridge that allows techniques developed in one field to be translated to another.**

Imaging is an umbrella term used for a large variety of techniques that aim to form a representation of an object's spatial distribution. The simplest and most common forms of optical imaging use a lens to reproduce the intensity of the light scattered from an object on an image plane where it can be measured by a multipixel detector array—a camera. This works because in free-space propagation, a lens can create a reliable one-to-one mapping between each point on the imaged plane and each point on the detector. However, if light is scattered during its propagation this relationship is broken: the light from each point on the object is spread to many camera pixels, and the quality of the image is degraded. How much the quality of the image degrades depends on how and how much of the light is scattered. This is dictated by the properties of the medium, and can be characterized by the medium's transport mean free path, $\ell_t$ (ref. [1]). For a collimated light beam, the fraction of light still unscattered after traversing a scattering medium of thickness $L$ will be given by the Lambert–Beer law: $e^{-L/\ell_t}$ (ref. [2]).

As shown in Fig. 1, at a distance $L<\ell_t$ only a small fraction of light has been scattered, and the reduction in imaging quality is minimal. However, at a distance $L\approx\ell_t$, a substantial fraction of the light has been scattered, resulting in a blurry background, obscuring the object features. Finally, for $L\gg\ell_t$ essentially all of the light has been scattered and the conventional image degrades to the point where no sharp object features can be seen (Fig. 1)[3].

Whether a sample is scattering or not also depends on the type of wave used for imaging. For example, soft tissues scatter visible light, but not X-rays or ultrasound. Similarly, concrete walls scatter (and absorb) light and sound, but affect radio-frequency waves much less. As a consequence, two direct approaches to avoid scattering are modifying the medium or the imaging modality. Examples include tissue clearing by chemical means[4] and the use of X-rays to image inside the body[5]. Despite the existence of techniques that turn scattering into a non-problem, there are situations where none of these options are viable. Such is the case when the medium cannot be altered, when ionizing radiation (such as X-rays) is undesired or when the contrast or resolution provided by the non-scattered waves is insufficient. For example, the non-microscopic resolution of ultrasound imaging cannot resolve cellular structures[6]. In this Review we describe the main techniques that have been developed to tackle scattering, with a focus on the recent developments in optical imaging, but with the goal of highlighting the fundamental similarities between different fields and approaches.

## Imaging by filtering out scattered light

In many instances of imaging in volumetric scattering media—particularly at depths below $\ell_t$—a small fraction of light remains unscattered. One option to improve imaging is therefore to use only this small portion of unscattered (or 'ballistic') light to form the image. This approach has the advantage that, because the light used for imaging was never disturbed, one can directly reconstruct very sharp images.

There are different approaches to separate the scattered and unscattered light. One option is to time-gate the light by sending short pulses to illuminate the scene and then measure only the light arriving at a given time. As the diffused background travels through many different paths, it is temporally broad, and a short time-gate preferentially selects the light that bounced back from the object but was otherwise unscattered. This approach has the additional advantage of providing a measurement of the distance, allowing a three-dimensional reconstruction, and is thus commonly used in light detection and ranging (LiDAR)[7]. For time-gating to work, the time gate has to be much shorter than the typical temporal spread of the signal. Time-gating can be achieved by using fast detectors, or by low-coherence interferometry using a short-temporal-coherence source, which is the basis for optical coherence tomography (OCT)[8].

A different approach to preferentially measure unscattered light is spatial gating, which aims to select the light that originated from a specific illuminated point in the medium. The idea is that when focused illumination and an imaging system are used, the scattered light would be spread over a large area in the detector plane, whereas the unscattered light would be concentrated around the imaged illumination point. This is the principle behind confocal microscopy[9]. Another effective approach for spatial gating is to use nonlinear signal generation mechanisms, such as harmonic frequency generation or multiphoton fluorescence excitation[10]. Multiphoton microscopy exploits the fact that nonlinear signals are preferentially generated at the focus, where the instantaneous intensity is the highest[11], and has recently achieved imaging at depths approaching $\ell_t$ (ref. [12]).

The main limitation of gating-based approaches are that there is always a small fraction of scattered light that incidentally underwent a path of exactly the same length and direction as the unscattered ballistic light and the intensity of the unscattered light decays exponentially with depth. Therefore, at sufficiently large imaging depths, the detected intensity of the unwanted scattered waves, which decay linearly with depth, will be higher than that of the desired unscattered waves[13]. Although the exact values depend on the details of the medium and specific technique, such 'filtering' approaches tend

[1]Physics and Astronomy Department, University of Exeter, Exeter, UK. [2]Department of Applied Physics, The Hebrew University of Jerusalem, Jerusalem, Israel. ✉e-mail: J.Bertolotti@exeter.ac.uk; orik@mail.huji.ac.il


**Fig. 1 | Imaging through fog as one example of optical imaging through complex media.** Fog is composed of small water droplets that scatter visible light, preventing the formation of a clear image. Imaging through a layer of fog thinner than a characteristic distance, $\ell_t$, known as the transport mean free path, will result in a slightly degraded image, but if the thickness of the fog layer, $L$, is much bigger than $\ell_t$, no image can be formed at all.

to work up to thicknesses comparable to $\ell_t$, and degrade quickly beyond it. To reach greater depths one must therefore use scattered light for imaging, rather than discard it.

## Imaging with scattered light

**The scattering matrix formalism.** When imaging at depths beyond $\ell_t$, one has no choice but to form the image from the (multiply) scattered light[14]. Since in nearly all practical optical imaging situations the light intensities involved are too low to induce a substantial nonlinear interactions outside the focus, light propagation in complex media can be considered linear. As a consequence, the scattered optical field measured after propagation through a complex medium is a linear sum of the medium's response to the field at each point in the input plane (Fig. 2a).

Formally, the propagation through a complex medium is described by a set of Green functions, $G(\mathbf{r}_{in}, t_{in}, \mathbf{r}_{out}, t_{out})$, connecting the input field at each position coordinate $\mathbf{r}_{in}$ and time $t_{in}$ (for example, the field at the target object plane, $E^{in}(\mathbf{r}_{in}, t_{in})$) with the output field at each output position coordinate, $\mathbf{r}_{out}$, at a time $t_{out}$ (for example, the field at the camera plane, $E^{out}(\mathbf{r}_{out}, t_{out})$). If the scattering medium response is time-invariant, the Green function depends only on $t = t_{out} - t_{in}$, and one can perform a Fourier transform with respect to time to obtain the complex-valued input–output relation at each angular frequency $\omega$: $G_\omega(\mathbf{r}_{in}, \mathbf{r}_{out})$. For simplicity, we will consider the case of monochromatic excitation, where the input–output relations are given by the single-frequency response: $E^{out}(\mathbf{r}_{out}) = \iint\!\!\iint G_\omega(\mathbf{r}_{in}, \mathbf{r}_{out}) E^{in}(\mathbf{r}_{in}) \mathrm{d}^3\mathbf{r}_{in}$.

In the spatial domain, the field can be decomposed into discrete spatial channels: $E_n(r)$ (with $n = 1 \ldots N$). Thus, the medium's Green functions can be discretized in space, and written as a single complex-valued matrix, $S$ (for each frequency $\omega$). This scattering matrix fully describes the medium response in both transmission and reflection (for a more detailed discussion, see ref. [15]). Each of its elements, $S_{m,n}$, describes the response at the $m$-th output mode for excitation of the $n$-th input mode (Fig. 2a,b). In the scattering matrix formalism, the output field is given by the matrix multiplication between the scattering matrix and the input field: $E^{out} = SE^{in}$; that is, $E^{out}_m = S_{m,n}E^{in}_n$.

Each scattering matrix column $n = 1 \ldots N$ thus gives the Green function (impulse response) of the medium to excitation by the input mode $n$ (Fig. 2b). One has the freedom to choose which basis to use for the field decomposition. Although the real-space and k (angular) space bases are two natural and common choices in optics, other bases (such as transmission eigenchannels[16,17], principal modes[18] or singular vectors[13]) sometimes provide valuable insights into the physics of the system. It is often useful to separate the scattering matrix into 'transmission' ($T$) and 'reflection' ($R$) matrices, describing the medium response in transmission and reflection, respectively.

As the scattering matrix formalism describes any linear transformation, it can also describe the wave propagation—for any kind of wave, not only light—from a target object to the image plane of any linear imaging system, taking into account both the complex medium and imaging optics. In optical imaging, the image formed by a single point source is known as the point spread function (PSF)[19]. The columns of the transmission matrix in the canonical basis thus represent the coherent (field amplitude) PSF of each point in the object plane. Figure 2c–k provides three representative numerical examples of transmission matrices for three common practical imaging scenarios. First, the ideal case of a well-designed isoplanatic optical system imaging through a non-scattering homogeneous medium (Fig. 2c–e). In this case, the imaging PSF is a high-contrast diffraction-limited spot, the transmission matrix in the canonical basis is a nearly diagonal matrix (that is, all points have the same PSF) and the formed image is a sharp diffraction-limited representation of the object. Second, atmospheric turbulence or an imperfect imaging system comes with smooth, large-scale inhomogeneities (compared with the wavelength) that produce low-order aberrations, resulting in a wider PSF with a possibly non-flat phase response (Fig. 2f–h). Finally, there is imaging through multiply scattering turbid media. Here, the field from each input point is scattered multiple times and the interference between the different paths generates a complex speckle pattern (Fig. 2i–k), with sharp bright and dark spots of diffraction-limited dimensions: $\sigma_x \approx \lambda/\mathrm{NA}$, where $\lambda$ is the wavelength, and NA is the numerical aperture[20].

While the transmission matrix of a complex medium is the result of multiple scattering, it is not a completely random matrix but, perhaps surprisingly, possesses inherent correlations[15].

The most widely exploited type of correlation for imaging is the so-called optical memory effect for angular speckle correlations, which represents the inherent tilt invariance (or isoplanatism) of scattering through media of finite thickness[21,22]. It can be expressed as a similarity in the structure of speckle patterns generated at the image plane by light that originates from nearby points at the object plane (Box 1). The memory-effect correlations are, in essence, correlations between the scattering matrix columns when represented in the appropriate basis—in the plane-wave basis for a bare scattering medium or the canonical basis of a focused imaging system, with the complex medium at its pupil. Figure 2k provides an example. The correlations are clearly visible as diagonal smears, signifying the shift invariance of the scattering PSF in this imaging configuration. The angular range of the memory effect is thus the same isoplanatic angle—also known as the isoplanatic patch—used in adaptive optics[23] and ultrasound imaging[24]. Indeed, the generality of the scattering matrix formalism is not only useful for analysing optical imaging approaches, but also allows it to be commonly used in other domains from ultrasound[24,25] to geophysics[26].

**Diffuse optical tomography.** When the goal is to only image relatively large object features compared with the imaging depth, at depths considerably larger than $\ell_t$, then low-resolution imaging is possible even if the scattering matrix is not explicitly known. In such a case, the amplitude of the average spatial envelope of the scattering PSF, neglecting interference (that is, the diffusive blurry halo) is well

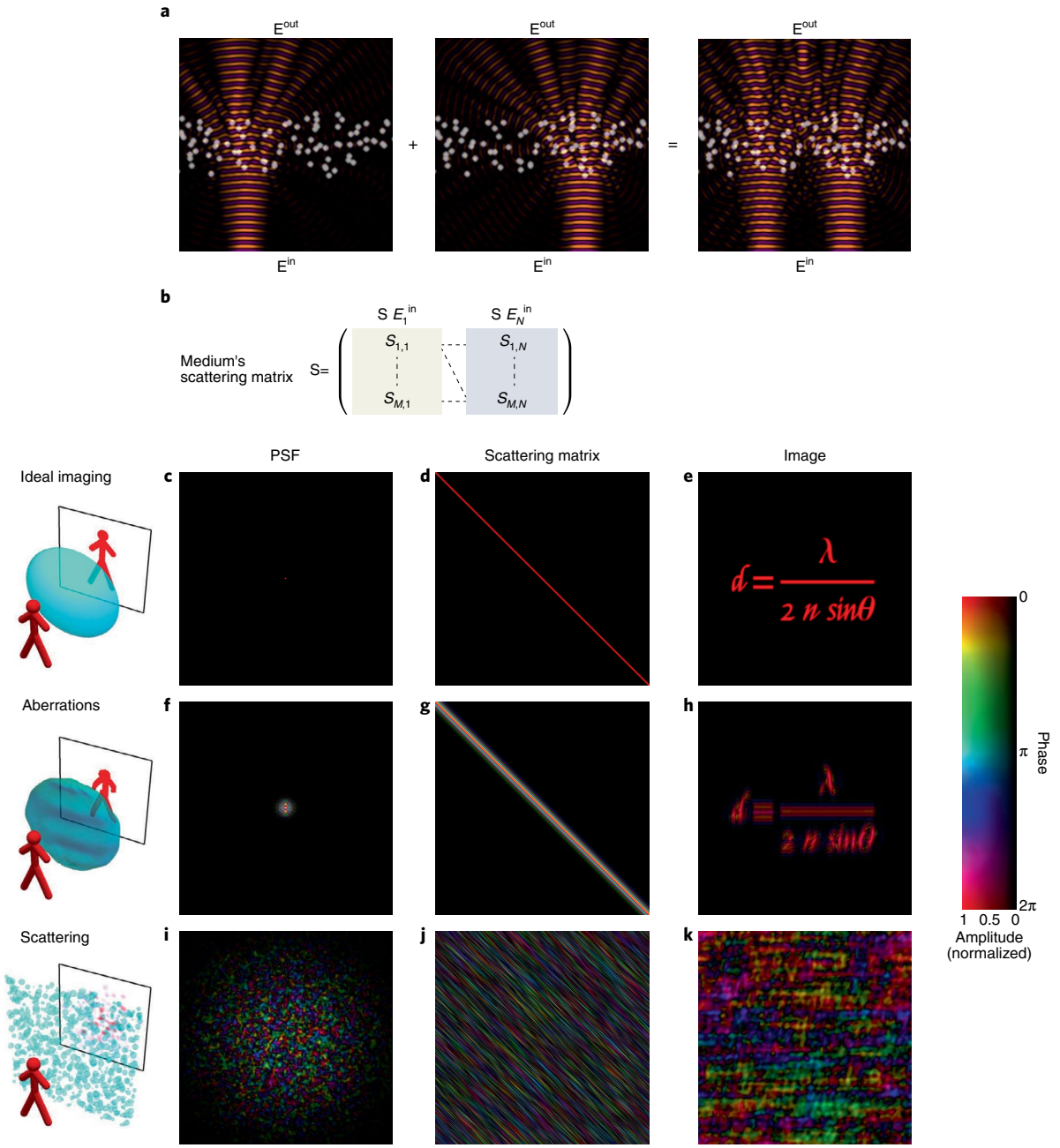


**Fig. 2 | Scattering-matrix formalism describing linear field propagation through complex media. a**, In most cases in optics, owing to the linearity of the problem the field produced by two sources is the sum of the fields produced by each source separately even after multiple scattering events (plotted here for a monochromatic case). **b**, For each monochromatic frequency, the scattered field is given by a matrix multiplication of the complex-valued scattering matrix $S$ with the input field: $E^{out} = SE^{in}$. Each column of $S$ is the response to an input (that is, a Green function). In the canonical basis, a column of $S$ is the complex field PSF. **c**–**k**, Numerical examples of the PSF (**c**,**f**,**i**), a slice of the $S$ matrix (**d**,**g**,**j**) and the resulting image (**e**,**h**,**k**) for several common imaging scenarios. **c**–**e**, An ideal, free-space, imaging system. **f**–**h**, Imaging through low-order aberrations, as in weak atmospheric turbulence. **i**–**k**, Imaging through a strongly scattering medium, where multiple scattering dominates.

described by a diffusion approximation[2]. If the geometry and scattering properties of the sample and system are known, it is possible to compute the resulting spatial distribution of the average intensity for each point of illumination[3]. In this fashion, a coarse-grained intensity-only transmission matrix of the medium that describes the forward problem can be constructed, and retrieval of deep-lying objects can be attempted by linear inversion. This is the principle behind diffuse optical tomography (DOT)[27]. As the coarse-grained forward diffusion problem effectively models scattering as blurring by a large Gaussian-like convolution kernel with a width of the order of the imaging depth, diffuse optical tomography can image inside strongly scattering media with a resolution of the order of the imaging depth[28].

**Computational imaging using a known transmission matrix.** In the scattering matrix framework, imaging in complex media can be interpreted as the reconstruction of the input field distribution, $E_{in}(x,y,z)$, from measured output fields (scattered light) distributions: $E_{out} = SE_{in}$. In principle, if the scattering matrix from the object plane to the image plane $S$ is known exactly, it is

**Box 1 | The optical memory effect**

Multiple scattering turns the imaging PSF into an apparently random speckle pattern. However, even after multiple scattering, the scattered light continues to contain correlations that can be exploited for imaging. One of these correlations that has recently found many uses in imaging is the so-called optical memory effect. A slight tilt of the illumination angle of a scattering medium results in an identical tilt of the speckle pattern at the medium's output facet, keeping its internal structure rather than completely randomizing it. (see panel a in the figure in this Box)[21,22]. One can understand the origin of this effect by considering that illuminating a point on a facet of a diffusive sample with a pencil-like beam results in a bright, diffusive blur only around the illumination point. Thus, the transmission matrix of the sample in the spatial position basis, $T_{r_{in},r_{out}}$, would be concentrated around the $\mathbf{r}_{in}$–$\mathbf{r}_{out}$ diagonal. The angular correlations of the memory effect become visible through inspecting this transmission matrix in the Fourier ($k_{in} - k_{out}$, where $k$ is the wave vector) basis (Fig. 2j)[22,113]. As the spatial extent of the diffusive blur grows with $L$ (the medium thickness), the angular correlation range scales as $\propto \lambda/L$.

An important consequence of the optical memory effect is that the PSFs from sources close to each other are similar, and thus the scattering from all sources within a given region (the isoplanatic patch) can be corrected with the knowledge of only a single PSF (see panel b in the figure in this Box). This forms the basis for most adaptive optics and several wavefront-shaping techniques (see the 'Wavefront shaping' section), as well as ultrasonic imaging[24]. Interestingly, the angular memory effect is also present in light propagation through multicore fibres, which opens the path to lensless diffraction-limited endoscopy (see panel c in the figure in this Box and the 'Imaging through optical fibres' section).

The major limitation of using the memory effect for imaging is its small field of view when imaging through thick samples. In such cases, the imaging field of view (FOV $\approx \frac{\lambda}{\pi L} d$, where $d$ is the distance between the object and the front facet of the scattering medium) is too small for most applications. Nonetheless, the FOV can be larger when imaging an object located at a large standoff distance from a thin scattering layer (i.e. in an 'eggshell' geometry). A similar result is obtained for non-line-of-sight imaging 'around-corners' using light reflected from a scattering wall, where the angular memory effect range in reflection is $\Delta\theta_{mem} \approx \lambda/(\pi \ell_t)$[22,69] (for alternative approaches of non-line-of-sight imaging see ref. [114]). The FOV can also be substantially larger when imaging through biological tissues at depths smaller than $\ell_t$ (ref. [115]) or when time-gated measurements are used[116].

Beyond angular correlations, additional inherent correlations are present in some scenarios. For example, anisotropic scattering in soft tissues of moderate thickness (compared with $\ell_t$) gives rise to speckle correlations for transverse translations of the incident wavefront as well[112,117].

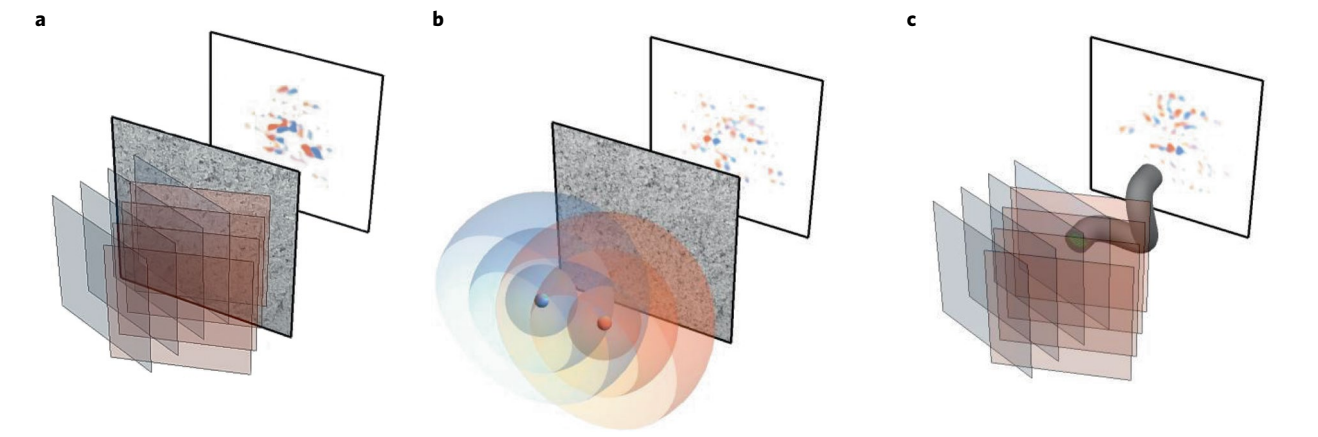


A correlation exists between the columns of the scattering matrix in the k-space basis (Fig. 2k). This correlation manifests as: **a**, Plane waves that illuminate the medium at similar angles and produce similar speckle patterns, with the same angular shift as the illumination beams. **b**, Light from adjacent points is scattered into similar speckle patterns, with an angular shift between them. **c**, The same effect is also present through multicore fibres, and in back-scattering from complex samples such as white-painted walls.

possible to calculate the input field using the matrix inverse $S^{-1}$. In practice, however, experiments are often limited to measuring only the transmission ($T$) or reflection ($R$) parts of $S$. Combined with measurement noise and absorption, this makes the exact inversion impossible. Nonetheless, it is possible to estimate the input field via the pseudo-inverse operator using a variety of well-established linear inverse problem approaches, such as the Moore–Penrose pseudo-inverse and Tikhonov regularization[29]. Improved reconstruction can be obtained using compressed-sensing reconstruction algorithms when priors on the object are available[30].

However, although the transmission matrix can be directly measured if one has access to both the input (object) plane and the output plane of the scattering medium[31], as was exploited in works that used a fixed random medium as a scattering lens[32,33], such 'invasive' access to the object plane is usually impossible in practice. Such is the case when non-invasive imaging through tissue is desired, and the imaging system cannot directly measure the single-pass transmission matrix from the object to the imaging system. A contemporary major challenge, and the focus of the remainder of this Review, lies in approaches that can estimate $T$ or $E_{in}$ from non-invasive measurements taken without accessing the object plane.

**Adaptive optics and wavefront shaping.** *Adaptive optics.* In the case where absorption is negligible, the scattering matrix is unitary, and can thus be interpreted as a rotation in a high-dimensional space[3]. If the full matrix is known or can be measured, scattering can be

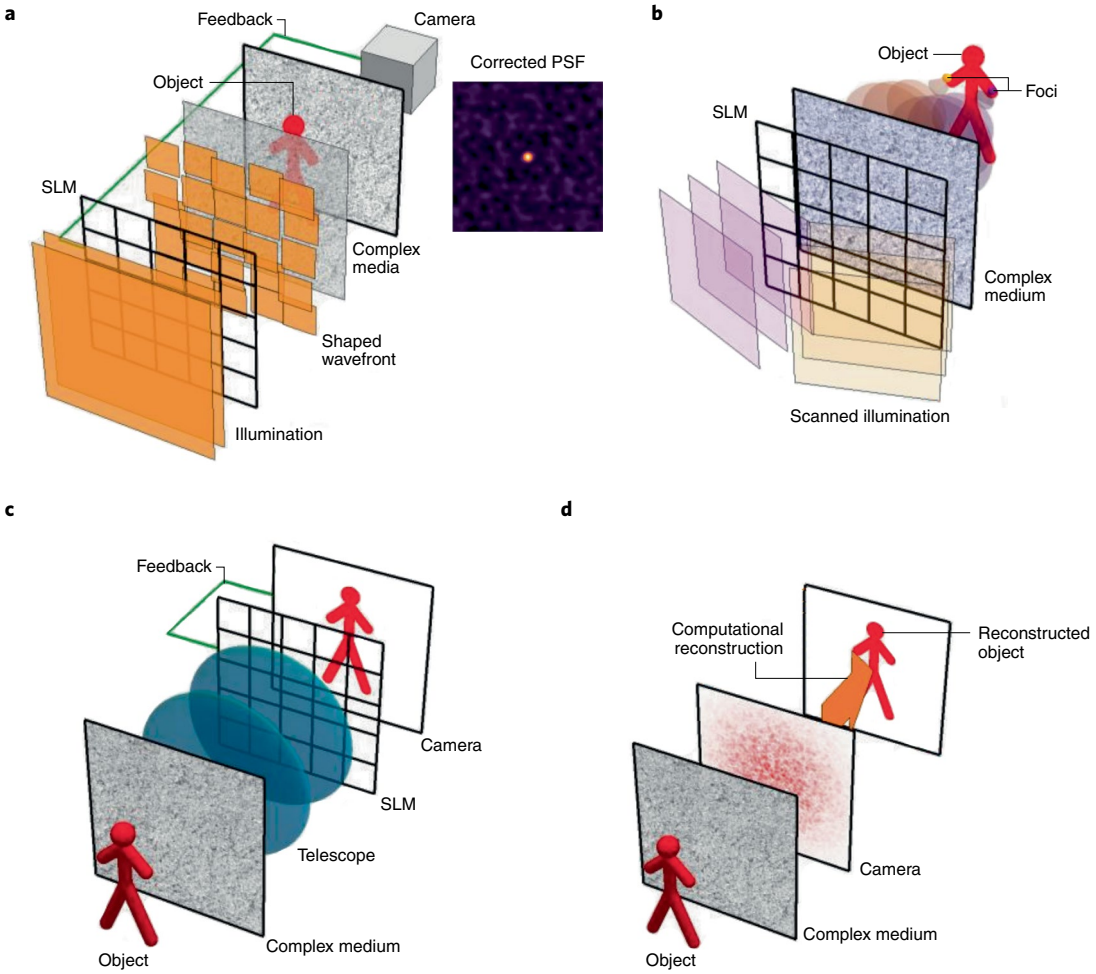


**Fig. 3 | Different approaches for imaging via wavefront shaping. a**, The illumination wavefront is shaped by an SLM such that its interference after scattering by the complex medium forms a sharp diffraction-limited focus on the target (see the inset), physically undoing scattering. The optimal focusing wavefront is found by feedback from a detector or camera, potentially utilizing optical or acoustical modulation techniques, or both. **b**, The memory effect allows simple scanning of the formed focus across all points within the isoplanatic patch by tilting the correction wavefront. **c**, Similarly, via Helmholtz reciprocity, a single wavefront correction can simultaneously correct all points within the memory effect FOV for wide-field imaging. **d**, Wide-field imaging can be performed computationally from scattered light measurements, without a physical correction.

inverted not just computationally, but also physically, by applying an equal and opposite rotation using a wavefront correcting device with a sufficient number of controllable elements (degrees of freedom, or modes). Such a device can be realized by deformable mirrors or spatial light modulators (SLMs). This is the principle for correcting low-order aberrations by adaptive optics, which was pioneered for astronomical observations[23] (Fig. 2f–h). Today it is possible to near-perfectly correct atmospheric distortions in astronomical observations[23] and isoplanatic sample-induced aberrations in microscopy[34], as long as the number of controllable elements is larger than the number of scattered modes. The wavefront correction is determined by either measuring the wavefront distortions of light originating from one or several points located behind the aberrating medium—these are called guide stars—or by varying the correction to optimize an image metric[34,35]. The correction can be extended beyond a single isoplatic patch with the help of multiple guide stars and multiple SLMs or deformable mirrors.

*Wavefront shaping.* When the number of scattered modes, $N_{\mathrm{modes}}$, increases beyond the number of controllable degrees of freedom, $N_{\mathrm{SLM}}$—for example, in deep-tissue imaging, where the number of scattered modes can easily exceed $10^6$—it becomes practically impossible to measure and correct all of the scattered modes. In this deep multiple-scattering regime, light forms complex speckle patterns (Fig. 2i) and the scattering matrix stops being even approximately diagonal (Fig. 2j). However, it is still possible to manipulate the scattered light to a useful degree and form a high-contrast diffraction-limited focus on the target by enhancing the intensity of a single speckle grain through constructive interference of the controlled modes (inset in Fig. 3b). Strikingly, even though $N_{\mathrm{SLM}} \ll N_{\mathrm{modes}}$, as long as the controlled scattered modes are independent, the intensity of the wavefront-corrected focus would be approximately $N_{\mathrm{SLM}}$ times higher than the average intensity of the residual speckle background, which remains due to the imperfect correction[36]. Since hundreds to $10^5$ modes are today routinely controlled with state-of-the-art SLMs, high-contrast focusing that can be effective for imaging can be obtained, and the imperfect correction manifests only in a lower contrast compared with perfect focusing (inset in Fig. 3b). This fact forms the basis for the field of optical wavefront shaping[37,38]. The border between adaptive optics and wavefront shaping is not sharply defined, and a continuum exists between these extremes, which includes relevant applications such as the correction of low-order aberrations without undoing scattering[34].

If the scattering matrix is known, the correction wavefront for maximizing the focused intensity at a point $r_m$ on the target is given by phase-conjugating the $m$th row of the scattering matrix (in the canonical basis): $E_n^{\mathrm{SLM,in}} = s_{m,n}^*$, where the asterisk indicates the complex conjugate. The output field at $r_m$ would then be $E_m = \sum_n s_{m,n} s_{m,n}^*$, and its intensity would be maximized because the phase-conjugated input effectively forms a matched filter for the scattering. However, when the scattering matrix is not known, the focusing SLM pattern can be found by an iterative search for the input wavefront that will form a bright focus after it is scattered. In its simplest implementation, directly—and invasively—measuring the intensity at the desired focus location[39] provides the feedback for the iterative optimization. A welcome side effect is that multiple scattering usually results in large scattering angles, which can be exploited to increase the effective NA of the focused wavefront, generating a focus with dimensions smaller than the diffraction limit of the optical system in free space[32,40]. In the near field, this scattering-lens effect can even be exploited for subwavelength focusing[32,33], as first demonstrated at microwave frequencies[41].

Devising schemes that provide non-invasive feedback for diffraction-limited focusing has been an area of intense research in recent years. The goal is to find the focusing wavefront with the help of measurements from detectors placed outside the sample (Fig. 3a). These state-of-the-art approaches make use of a large variety of physical mechanisms and computational methods[14]. Exploiting nonlinear signal generation mechanisms, such as multiphoton excitation of fluorescence or harmonic generation, allows diffraction-limited focusing by optimizing the total scattered nonlinear signal[42–45]. In the case of linear incoherent signal generation, such as fluorescence, using the scattered light image contrast as feedback for wavefront shaping can lead to focusing[46,47], because when light is focused to a single point, the scattered fluorescence pattern has maximal contrast. Similarly, the correction wavefront needed to obtain a sharp focus can be non-invasively found by directly optimizing an image contrast metric[48]. When the signal originates from a relatively small number of fluorescent emitters, non-negative matrix factorization of a matrix containing measured scattered fluorescence patterns allows non-invasive focusing[49]. In the case of spatially coherent signals, the spatial autocorrelation of the scattered light pattern can be used as a feedback mechanism for focusing, exploiting the memory effect[50].

Non-invasive focusing can also be obtained by computational decomposition of the reflection matrix, using either singular value decomposition[13,51] or more advanced computational algorithms that aim to decompose the scattering at the excitation and detection paths[52]. If the structure of the scattering medium can be measured or modelled, the correction wavefront can be estimated computationally[53].

The major drawback of iterative optimization or matrix-based approaches is that they require a large number of sequential measurements—equal to or larger than the number of controllable modes—to determine the focusing wavefront. This limitation can be sidestepped by leveraging the time-reversal symmetry of multiple scattering: if the multiply scattered wave produced by a point source is measured and time-reversed, it will propagate back to focus at the original source position, which allows focusing using a single-shot wavefront measurement. This was first demonstrated for multiple scattering compensation in acoustics by time-reversal mirrors[24] and in optics by nonlinear crystals[54]. In recent years, digital phase conjugation using computer-controlled SLMs has replaced the analogue nonlinear crystal-based approach, as digital phase conjugation offers simplicity and flexibility not only for coherent scattered light[55], but also using nonlinear[56] and fluorescence[57] signals. The downside of direct phase-conjugation is the requirement for a point source 'guide star' at the target plane.

Optical imaging in soft tissues can leverage the fact that acoustic waves essentially do not experience scattering to produce guide stars on demand. Such ultrasound-mediated guidance can be realized in two ways: either via ultrasonic detection of acoustic signals generated by the photo-acoustic effect, following optical absorption[58], or using localized acousto-optic modulation of light by focused ultrasound[59]. Similarly to all-optical techniques, focusing can be achieved via iterative optimization[60,61], by computational analysis of a photoacoustically or acousto-optically measured scattering matrix[62,63] or via phase conjugation[59]. The major drawback of acousto-optic and photo-acoustic guide stars is that their dimensions are dictated by the acoustic wavelength—orders of magnitude larger than the optical diffraction limit. Reducing the size of the acousto-optically guided focus can be effectively achieved by iterative phase conjugation[64], whereby the phase conjugation and acousto-optic modulation process is repeated several times, shrinking the size of the focus in each iteration. Mathematically, iterative phase conjugation is equivalent to raising the scattering matrix to the power of the number of iterations. Repeating the process is therefore equivalent to finding the highest singular value of the scattering matrix. The same result can thus be obtained by injecting the first singular vector of the scattering matrix, as was first realized in acoustics[65], and put to use in all-optical[51] and acousto-optical[63,66] approaches.

When non-monochromatic light focusing is required (for example, when ultrashort pulses are used for multiphoton excitation) scattering may also induce temporal distortions, which will require correction in addition to the spatial distortions. Strikingly, temporal control can be obtained by controlling only the spatial degrees of freedom, as a result of the spatiotemporal coupling of multiple scattering[67].

*From focusing to imaging.* The ability to form a focus by itself is not enough for imaging. However, it may enable imaging if the focus can be scanned over a sufficiently large FOV, effectively realizing a laser scanning imaging system. Such scanning is indeed directly possible within the limited FOV of the optical memory effect[68] (Fig. 3b and Box 1). As an alternative to focus scanning, one can exploit the fact that, in most instances in optics, Helmholtz reciprocity allows the source and detector to be exchanged without changing the result. As a result, the memory effect also means that all the points within the isoplanatic patch can be corrected simultaneously by placing the SLM in the detection path instead of the illumination path. Thus, if the wavefront correction for a point is known, it is possible to use it to perform wide-field single-shot imaging[69] (Fig. 3c).

*Computational imaging through complex media.* A very promising direction for imaging that does not require physical correction of scattering and can be implemented without a wavefront shaping device is the use of computational image reconstruction. As suggested by Freund three decades ago[22], memory effect-based imaging can be possible even without a physical correction device. Most importantly, the memory-effect also allows imaging without knowledge or measurement of the scattering matrix. The first realization in multiply scattering media was demonstrated by scanning unknown, but correlated, speckle patterns over a fluorescence target (see panel a in the figure in Box 1) and recording the total fluorescence signal excited by each pattern[70]. The measured intensity of the fluorescence signal is proportional to the overlap between the speckle pattern and the target object, and its intensity as a function of scanning angle therefore provides the convolution of the object with the unknown speckle pattern. As the spatial autocorrelation of a speckle pattern is a diffraction-limited peak[20], the autocorrelation of the scan trace provides the target object autocorrelation, and the object image can be computationally reconstructed via phase retrieval[71] or bi-spectrum[72] reconstruction techniques adapted from astronomy. Thanks to Helmholtz reciprocity, a similar measurement can be performed in a single shot[45,73] (Fig. 3c), bringing Labeyrie's stellar speckle interferometry[74] from astronomy to complex media.

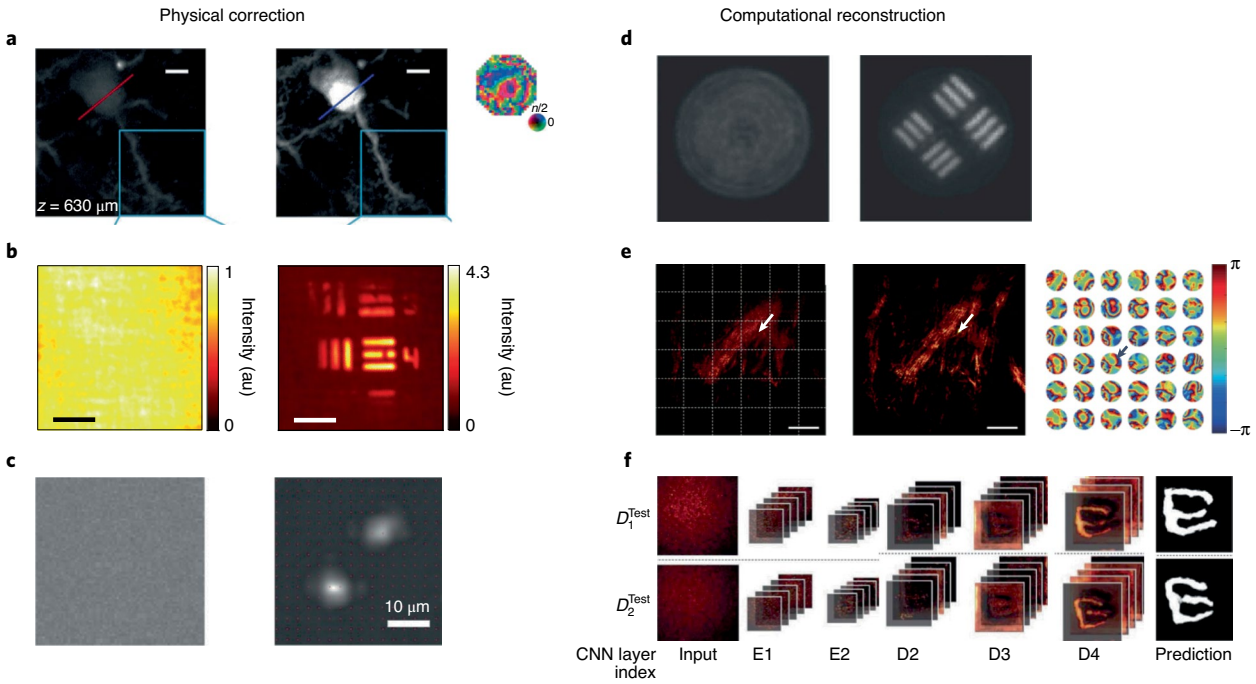


**Fig. 4 | Examples of diffraction-limited images obtained non-invasively through complex media with various approaches. a–c**, Physical correction of scattering using wavefront shaping, where the correction is found by nonlinear signal optimization[44] (**a**), image-metric optimization[48] (**b**) or singular value decomposition of acousto-optically tagged speckle patterns[66] (**c**). **d–f**, Computational reconstruction via estimation of a multimode fibre transmission matrix from physical fibre parameters[100] (**d**), decomposition of the time-gated reflection matrix[112] (**e**), and deep learning of speckle correlations[88] (**f**). E1–D4 are visualizations of the intermediate activation maps in several selected layers of the convolutional neural network (CNN). The left images in all panels are the conventionally captured, uncorrected images. The right images in **a–d**,**f** and the middle panel in **e** are the corrected images. The inset in **a** and right part of **e** display the applied wavefront corrections. Scale bars: 5 μm (**a**,**e**), 100 μm (**b**). Figure reproduced with permission from: **a**, ref. [44], The Optical Society; **b**, ref. [48], AAAS CC BY-NC 4.0; **c**, ref. [66], Springer Nature Limited; **d**, ref. [100], Springer Nature Limited; **e**, ref. [112] under a Creative Commons license CC BY 4.0; **f**, ref. [88], The Optical Society.

The FOV limitation of the memory effect can be overcome by stitching multiple measurements, with each measurement imaging a FOV smaller than the isoplanatic patch size. This was recently demonstrated by decomposition of the reflection matrix to several isoplanatic corrections[25,75], non-negative matrix factorization of the fluorescence scattering matrix[49] and sequential acousto-optic modulation of small isoplanatic patches[76]. Such advanced computational reconstructions not only allow a wider FOV, but also provide a more stable convergence compared with iterative phase retrieval.

Computational reconstruction approaches have also been put forwards to improve the resolution of acousto-optic and photo-acoustic tomographic techniques. Random dynamic speckle illumination can improve the imaging fidelity and resolution of photo-acoustic and acousto-optic tomography[77–79], as randomly fluctuating speckle grains allow the adaptation of super-resolution optical fluctuation imaging (SOFI)[80] to ultrasound-mediated imaging. Flow-induced fluctuations were also utilized for super-resolved photoacoustics, either via SOFI[81] or by localization of flowing absorbers[82–85]. These approaches surpass the acoustic resolution and allow a very wide FOV but generally do not reach the optical diffraction limit.

Deep-learning neural-network-based approaches for imaging using scattered light are still in their infancy, but carry great potential to improve the reconstruction fidelity while alleviating the requirements for exact modelling, the number of measurements and the accuracy and stability of the optical set-up. Similar to scattering matrix-based approaches[29], deep learning can be applied to solve the inverse problem of recovering the object information from a dataset of scattered light measurements[86–89], effectively incorporating learned regularization, better estimation of the scattering matrix and generalization of speckle correlations. However, because coherent light propagation and speckle patterns are not present in most common imaging problems, the conventional network architectures used in those situations may not be optimal for imaging in complex media. To go beyond the performance of non-deep-learning scattering matrix-based approaches, recent deep-learning works utilized a hybrid model-based or physics-informed network architecture[90], allowing not just the object information, but also the parameters of the optical set-up to be retrieved[91,92].

## Imaging through optical fibres

While one would always prefer imaging techniques to be non-invasive, this is not always possible. For imaging at very large depths, absorption ultimately limits information transmission and minimally invasive techniques (such as endoscopy) that are based on the insertion of a small-diameter probe to bypass scattering and absorption are used[93]. Fibre-based microendoscopes are a common solution. However, their diameter is typically larger than the imaged FOV due to the use of lenses or scanners at the distal fibre end or aberrations in graded-index rod lenses. A lensless endoscope, based on a small-diameter bare fibre, is thus a highly attractive solution.

As the scattering matrix formalism also describes light propagation through optical fibres, the same techniques used for focusing and imaging in complex media can be employed to realize lensless bare-fibre endoscopes. The reason that the scattering matrix of the fibre is required to reconstruct the optical field at the distal end from its measurements at the proximal end is that multimode propagation through a fibre—be it a multimode fibre or a multicore fibre—induces different phase accumulation for the different

modes, resulting in a complex speckle pattern similar to the one produced by multiple scattering[94].

While an image was first projected through a multimode fibre in the 1960s[95], measuring the transmission matrix of a fibre only became feasible with the advent of digital holography and wavefront shaping[96,97]. As in complex media, imaging can be performed computationally[98] or by scanning a wavefront-shaped focus[97,99]. However, unless the fibre is kept static (for example, fixed inside a stiff needle) its transmission matrix will change upon any bending or even temperature change[100]. Thus, non-invasive in situ calibration is a requirement for imaging through flexible fibres. As in complex media, non-invasive focusing and imaging are possible by using a nonlinear guide star[101], decomposing the reflection matrix[102] or by placing engineered reflecting layers next to the distal fibre tip[103,104]. Imaging in multimode fibres can be performed through knowledge of the entire matrix or partial knowledge of the transmission matrix by exploiting the rotational memory-effect present in cylindrically symmetric (unperturbed) fibres[105,106]. Alternatively, if the precise structure and bending of the fibre are known, it is possible to predict the changes in the transmission matrix[100]. Designing fibres with reduced sensitivity to bending is also an ongoing effort[107,108].

Fibre bundles composed of thousands of individual few-mode fibres (Fig. 3c) are especially interesting systems, as the small coupling between cores leads to a propagation that is analogous to a thin scattering layer (or diffuser). They thus possess the conventional angular memory effect, and it is possible to exploit it in similar fashions as for scattering media[99,109]. It is worth mentioning that, although single-mode fibres have only one spatial degree of freedom, imaging information can nonetheless be transmitted in their spectral (or equivalently, temporal) degrees of freedom by placing a spatiospectral encoder at the distal end of the fibre[110]. As in scattering media, deep-learning-based approaches have found use in computational imaging through fibres and are the subject of intense research[87,111].

Figure 4 presents some recent results for diffraction-limited non-invasive imaging through complex media, either via physical correction (Fig. 4a–c) or computational reconstruction (Fig. 4d–f).

## Discussion

Scattering in complex media makes imaging information difficult to retrieve. Until recently this was an intractable problem, but advances in the available technology, computational approaches and our understanding of multiple scattering have led to a proliferation of new techniques and surprising results. These approaches have emerged from different communities, and are often useful in different regimes. As a result, the nomenclature, formalism and descriptions may vary considerably from one community to another. This may intimidate newcomers, but, as is often the case, the various techniques are more similar than they seem to be on the surface. The scattering matrix formalism provides a unified framework to describe the different approaches, highlighting the similarities and encouraging communication between fields.

The topic of imaging in complex media has evolved rapidly, producing many astonishing results, but with a few exceptions these results have not yet percolated to the wider imaging community. One major reason for this is that many approaches only work well in some very specific circumstances, which those working on real-world applications may find too restrictive. Therefore, a major challenge that needs to be tackled in the near future is how to overcome this gap. This will necessitate technological advancements, including faster measurements and more sensitive detectors, to allow the measurement of the $S$ matrix within the sample decorrelation time, but mostly it will require ideas from fields that approach the problem from different directions to be combined.

That said, it is unlikely that a universal technique, able to perform imaging in all scattering regimes, will ever be found. What is more likely is that a number of techniques will be developed, each suitable for a specific real-world situation—making a unified framework and ease of communication between fields even more important.

Received: 31 January 2022; Accepted: 1 July 2022;
Published online: 8 September 2022

## References

1. Sheng, P. *Introduction to Wave Scattering, Localization and Mesoscopic Phenomena* (Springer, 2010).
2. Akkermans, E. & Montambaux, G. *Mesoscopic Physics of Electrons and Photons* (Cambridge Univ. Press, 2007).
3. Carminati, R. & Schotland, J. C. *Principles of Scattering and Transport of Light* (Cambridge Univ. Press, 2021).
4. Richardson, D. S. & Lichtman, J. W. Clarifying tissue clearing. *Cell* **162**, 246–257 (2015).
5. Chen, H., Rogalski, M. M. & Anker, J. N. Advances in functional X-ray imaging techniques and contrast agents. *Phys. Chem. Chem. Phys.* **14**, 13469–13486 (2012).
6. Szabo, T. L. *Diagnostic Ultrasound Imaging: Inside Out* (Elsevier, 2014).
7. McCarthy, A. et al. Long-range time-of-flight scanning sensor based on high-speed time-correlated single-photon counting. *Appl. Opt.* **48**, 6241–6251 (2009).
8. Huang, D. et al. Optical coherence tomography. *Science* **254**, 1178–1181 (1991).
9. Pawley, J. (ed.) *Handbook Of Biological Confocal Microscopy* (Springer, 2006).
10. Zipfel, W. R., Williams, R. M. & Webb, W. W. Nonlinear magic: multiphoton microscopy in the biosciences. *Nat. Biotechnol.* **21**, 1369–1377 (2003).
11. Theer, P. & Denk, W. On the fundamental imaging-depth limit in two-photon microscopy. *J. Opt. Soc. Am. A* **23**, 3139–3149 (2006).
12. Horton, N. G. et al. In vivo three-photon microscopy of subcortical structures within an intact mouse brain. *Nat. Photon.* **7**, 205–209 (2013).
13. Badon, A. et al. Smart optical coherence tomography for ultra-deep imaging through highly scattering media. *Sci. Adv.* **2**, e1600370 (2016).
14. Yoon, S. et al. Deep optical imaging within complex scattering media. *Nat. Rev. Phys.* **2**, 141–158 (2020).
15. Cao, H., Mosk, A. P. & Rotter, S. Shaping the propagation of light in complex media. *Nat. Phys*. https://doi.org/10.1038/s41567-022-01677-x (2022).
16. Choi, W., Mosk, A. P., Park, Q.-H. & Choi, W. Transmission eigenchannels in a disordered medium. *Phys. Rev. B* **83**, 134207 (2011).
17. Yilmaz, H., Hsu, C. W., Yamilov, A. & Cao, H. Transverse localization of transmission eigenchannels. *Nat. Photon.* **13**, 352–358 (2019).
18. Carpenter, J., Eggleton, B. J. & Schröder, J. Observation of Eisenbud-Wigner-Smith states as principal modes in multimode fibre. *Nat. Photon.* **9**, 751–757 (2015).
19. Goodman, J. W. *Introduction to Fourier Optics* (Roberts & Company, 2005).
20. Goodman, J. W. *Speckle Phenomena in Optics: Theory and Applications* (SPIE, 2020).
21. Feng, S., Kane, C., Lee, P. A. & Stone, A. D. Correlations and fluctuations of coherent wave transmission through disordered media. *Phys. Rev. Lett.* **61**, 834–837 (1988).
22. Freund, I. Looking through walls and around corners. *Phys. A* **168**, 49–65 (1990).
23. Davies, R. & Kasper, M. Adaptive optics for astronomy. *Annu. Rev. Astron. Astrophys.* **50**, 305–351 (2012).
24. Fink, M. et al. Time-reversed acoustics. *Rep. Prog. Phys.* **63**, 1933–1995 (2000).
25. Badon, A. et al. Distortion matrix concept for deep optical imaging in scattering media. *Sci. Adv.* **6**, eaay7170 (2020).
26. Blondel, T., Chaput, J., Derode, A., Campillo, M. & Aubry, A. Matrix approach of seismic imaging: application to the Erebus volcano, Antarctica. *J. Geophys. Res. Solid Earth* **123**, 10936–10950 (2018).
27. Arridge, S. Methods in diffuse optical imaging. *Phil. Trans. R. Soc. A* **369**, 4558–486 (2011).
28. Gibson, A., Hebden, J. & Arridge, S. Recent advances in diffuse optical imaging. *Phys. Med. Biol.* **50**, R1 (2005).
29. Popoff, S., Lerosey, G., Fink, M., Boccara, A. C. & Gigan, S. Image transmission through an opaque material. *Nat. Commun.* **1**, 81 (2010).
30. Liutkus, A. et al. Imaging with nature: Compressive imaging using a multiply scattering medium. *Sci. Rep.* **4**, 5552 (2014).
31. Popoff, S. M. et al. Measuring the transmission matrix in optics: an approach to the study and control of light propagation in disordered media. *Phys. Rev. Lett.* **104**, 100601 (2010).

32. van Putten, E. G. et al. Scattering lens resolves sub-100 nm structures with visible light. *Phys. Rev. Lett.* **106**, 193905 (2011).
33. Choi, Y. et al. Overcoming the diffraction limit using multiple light scattering in a highly disordered medium. *Phys. Rev. Lett.* **107**, 023902 (2011).
34. Ji, N. Adaptive optical fluorescence microscopy. *Nat. Methods* **14**, 374–380 (2017).
35. Wu, T., Berto, P. & Guillon, M. Reference-less complex wavefields characterization with a high-resolution wavefront sensor. *Appl. Phys. Lett.* **118**, 251102 (2021).
36. Vellekoop, I. M. & Mosk, A. P. Focusing coherent light through opaque strongly scattering media. *Opt. Lett.* **32**, 2309–2311 (2007).
37. Vellekoop, I. M. & Mosk, A. P. Universal optimal transmission of light through disordered materials. *Phys. Rev. Lett.* **101**, 120601 (2008).
38. Mosk, A. P., Lagendijk, A., Lerosey, G. & Fink, M. Controlling waves in space and time for imaging and focusing in complex media. *Nat. Photon.* **6**, 283–292 (2012).
39. Vellekoop, I. Feedback-based wavefront shaping. *Opt. Express* **23**, 12189–12206 (2015).
40. Yilmaz, H. et al. Speckle correlation resolution enhancement of wide-field fluorescence imaging. *Optica* **2**, 424–429 (2015).
41. Lerosey, G., de Rosny, J., Tourin, A. & Fink, M. Focusing beyond the diffraction limit with far-field time reversal. *Science* **315**, 1120–1122 (2007).
42. Tang, J., Germain, R. & Cui, M. Superpenetration optical microscopy by iterative multiphoton adaptive compensation technique. *Proc. Natl Acad. Sci. USA* **109**, 8434–8439 (2012).
43. Papadopoulos, I. et al. Dynamic conjugate F-SHARP microscopy. *Light Sci. Appl.* **9**, 110 (2020).
44. Berlage, C. et al. Deep tissue scattering compensation with three-photon F-SHARP. *Optica* **8**, 1613–1619 (2021).
45. Katz, O., Heidmann, P., Fink, M. & Gigan, S. Non-invasive single-shot imaging through scattering layers and around corners via speckle correlations. *Nat. Photon.* **8**, 784–790 (2014).
46. Boniface, A., Blochet, B., Dong, J. & Gigan, S. Noninvasive light focusing in scattering media using speckle variance optimization. *Optica* **6**, 1381–1385 (2019).
47. Daniel, A., Oron, D. & Silberberg, Y. Light focusing through scattering media via linear fluorescence variance maximization, and its application for fluorescence imaging. *Opt. Express* **27**, 21778–21786 (2019).
48. Yeminy, T. & Katz, O. Guidestar-free image-guided wavefront shaping. *Sci. Adv.* **7**, eabf5364 (2021).
49. Boniface, A., Dong, J. & Gigan, S. Non-invasive focusing and imaging in scattering media with a fluorescence-based transmission matrix. *Nat. Commun.* **11**, 6154 (2020).
50. Stern, G. & Katz, O. Noninvasive focusing through scattering layers using speckle correlations. *Opt. Lett.* **44**, 143–146 (2019).
51. Popoff, S. M. et al. Exploiting the time-reversal operator for adaptive optics, selective focusing, and scattering pattern analysis. *Phys. Rev. Lett.* **107**, 263901 (2011).
52. Kang, S. et al. Imaging deep within a scattering medium using collective accumulation of single-scattered waves. *Nat. Photon.* **9**, 253–258 (2015).
53. Thendiyammal, A., Osnabrugge, G., Knop, T. & Vellekoop, I. M. Model-based wavefront shaping microscopy. *Opt. Lett.* **45**, 5101–5104 (2020).
54. Yaqoob, Z., Psaltis, D., Feld, M. & Yang, C. Optical phase conjugation for turbidity suppression in biological samples. *Nat. Photon.* **2**, 110–115 (2008).
55. Cui, M. & Yang, C. Implementation of a digital optical phase conjugation system and its application to study the robustness of turbidity suppression by phase conjugation. *Opt. Express* **18**, 3444–3455 (2010).
56. Hsieh, C., Pu, Y., Grange, R., Laporte, G. & Psaltis, D. Imaging through turbid layers by scanning the phase conjugated second harmonic radiation from a nanoparticle. *Opt. Express* **18**, 20723–20731 (2010).
57. Vellekoop, I., Cui, M. & Yang, C. Digital optical phase conjugation of fluorescence in turbid tissue. *Appl. Phys. Lett.* **101**, 081108 (2012).
58. Xu, M. & Wang, L. V. Photoacoustic imaging in biomedicine. *Rev. Sci. Instrum.* **77**, 041101 (2006).
59. Xu, X., Liu, H. & Wang, L. V. Time-reversed ultrasonically encoded optical focusing into scattering media. *Nat. Photon.* **5**, 154–157 (2011).
60. Kong, F. et al. Photoacoustic-guided convergence of light through optically diffusive media. *Opt. Lett.* **36**, 2053–2055 (2011).
61. Lai, P., Wang, L., Tay, J. W. & Wang, L. V. Photoacoustically guided wavefront shaping for enhanced optical focusing in scattering media. *Nat. Photon.* **9**, 126–132 (2015).
62. Chaigne, T. et al. Controlling light in scattering media non-invasively using the photoacoustic transmission matrix. *Nat. Photon.* **8**, 58–64 (2014).
63. Katz, O., Ramaz, F., Gigan, S. & Fink, M. Controlling light in complex media beyond the acoustic diffraction-limit using the acousto-optic transmission matrix. *Nat. Commun.* **10**, 717 (2019).
64. Si, K., Fiolka, R. & Cui, M. Breaking the spatial resolution barrier via iterative sound-light interaction in deep tissue microscopy. *Sci. Rep.* **2**, 748 (2012).
65. Prada, C., Manneville, S., Spoliansky, D. & Fink, M. Decomposition of the time reversal operator: detection and selective focusing on two scatterers. *J. Acoust. Soc. Am.* **99**, 2067–2076 (1996).
66. Judkewitz, B., Wang, Y. M., Horstmeyer, R., Mathy, A. & Yang, C. Speckle-scale focusing in the diffusive regime with time reversal of variance-encoded light (TROVE). *Nat. Photon.* **7**, 300–305 (2013).
67. Aulbach, J., Gjonaj, B., Johnson, P., Mosk, A. & Lagendijk, A. Control of light transmission through opaque scattering media in space and time. *Phys. Rev. Lett.* **106**, 103901 (2011).
68. Vellekoop, I. & Aegerter, C. Scattered light fluorescence microscopy: imaging through turbid layers. *Opt. Lett.* **35**, 1245–1247 (2010).
69. Katz, O., Small, E. & Silberberg, Y. Looking around corners and through thin turbid layers in real time with scattered incoherent light. *Nat. Photon.* **6**, 549–553 (2012).
70. Bertolotti, J. et al. Non-invasive imaging through opaque scattering layers. *Nature* **491**, 232–234 (2012).
71. Fienup, J. R. Reconstruction of an object from the modulus of its Fourier transform. *Opt. Lett.* **3**, 27–29 (1978).
72. Wu, T., Katz, O., Shao, X. & Gigan, S. Single-shot diffraction-limited imaging through scattering layers via bispectrum analysis. *Opt. Lett.* **41**, 5003–5006 (2016).
73. Hofer, M., Soeller, C., Brasselet, S. & Bertolotti, J. Wide field fluorescence epi-microscopy behind a scattering medium enabled by speckle correlations. *Opt. Express* **26**, 9866–9881 (2018).
74. Labeyrie, A. Attainment of diffraction limited resolution in large telescopes by Fourier analysing speckle patterns in star images. *Astron. Astrophys.* **6**, 85 (1970).
75. Kang, S. et al. High-resolution adaptive optical imaging within thick scattering media using closed-loop accumulation of single scattering. *Nat. Commun.* **8**, 2157 (2017).
76. Rosenfeld, M. et al. Acousto-optic ptychography. *Optica* **8**, 936–943 (2021).
77. Gateau, J., Chaigne, T., Katz, O., Gigan, S. & Bossy, E. Improving visibility in photoacoustic imaging using dynamic speckle illumination. *Opt. Lett.* **38**, 5188–5191 (2013).
78. Chaigne, T. et al. Super-resolution photoacoustic fluctuation imaging with multiple speckle illumination. *Optica* **3**, 54–57 (2016).
79. Doktofsky, D., Rosenfeld, M. & Katz, O. Acousto optic imaging beyond the acoustic diffraction limit using speckle decorrelation. *Commun. Phys.* **3**, 5 (2020).
80. Dertinger, T., Colyer, R., Iyer, G., Weiss, S. & Enderlein, J. Fast, background-free, 3D super-resolution optical fluctuation imaging (SOFI). *Proc. Natl Acad. Sci. USA* **106**, 22287–22292 (2009).
81. Chaigne, T., Arnal, B., Vilov, S., Bossy, E. & Katz, O. Super-resolution photoacoustic imaging via flow-induced absorption fluctuations. *Optica* **4**, 1397–1404 (2017).
82. Dean-Ben, X. L. & Razansky, D. Localization optoacoustic tomography. *Light Sci. Appl.* **7**, 18004 (2018).
83. Kim, J. et al. Super-resolution localization photoacoustic microscopy using intrinsic red blood cells as contrast absorbers. *Light Sci. Appl.* **8**, 103 (2019).
84. Zhang, P., Li, L., Lin, L., Shi, J. & Wang, L. V. In vivo superresolution photoacoustic computed tomography by localization of single dyed droplets. *Light. Sci. Appl.* **8**, 36 (2019).
85. Vilov, S., Arnal, B. & Bossy, E. Overcoming the acoustic diffraction limit in photoacoustic imaging by the localization of flowing absorbers. *Opt. Lett.* **42**, 4379–4382 (2017).
86. Li, S., Deng, M., Lee, J., Sinha, A. & Barbastathis, G. Imaging through glass diffusers using densely connected convolutional networks. *Optica* **5**, 803–813 (2018).
87. Caramazza, P., Moran, O., Murray-Smith, R. & Faccio, D. Transmission of natural scene images through a multimode fibre. *Nat. Commun.* **10**, 2029 (2019).
88. Li, Y., Xue, Y. & Tian, L. Deep speckle correlation: a deep learning approach toward scalable imaging through scattering media. *Optica* **5**, 1181–1190 (2018).
89. Li, Y., Cheng, S., Xue, Y. & Tian, L. Displacement-agnostic coherent imaging through scatter with an interpretable deep neural network. *Opt. Express* **29**, 2244–2257 (2021).
90. Monakhova, K. et al. Learned reconstructions for practical mask-based lensless imaging. *Opt. Express* **27**, 28075–28090 (2019).
91. Matthès, M. W., Bromberg, Y., de Rosny, J. & Popoff, S. M. Learning and avoiding disorder in multimode fibers. *Phys. Rev. X* **11**, 021060 (2021).
92. Gigan, S. Imaging and computing with disorder. *Nat. Phys.* https://doi.org/10.1038/s41567-022-01681-1 (2022).
93. Gu, M., Bao, H. & Kang, H. Fibre-optical microendoscopy. *J. Microsc.* **254**, 13–18 (2014).
94. Okamoto, K. *Fundamentals of Optical Waveguides* (Elsevier, 2005).

95. Spitz, E. & Werts, A. Transmission des images à travers une fibre optique. *Comptes Rendus Hebd. Des. Seances De. L Acad.Des. Sci. Ser. B* **264**, 1015 (1967).
96. Di Leonardo, R. & Bianchi, S. Hologram transmission through multi-mode optical fibers. *Opt. Express* **19**, 247–254 (2010).
97. Čižmár, T. & Dholakia, K. Exploiting multimode waveguides for pure fibre-based imaging. *Nat. Commun.* **3**, 1027 (2012).
98. Choi, Y. et al. Scanner-free and wide-field endoscopic imaging by using a single multimode optical fiber. *Phys. Rev. Lett.* **109**, 203901 (2012).
99. Andresen, E. R., Bouwmans, G., Monneret, S. & Rigneault, H. Toward endoscopes with no distal optics: video-rate scanning microscopy through a fiber bundle. *Opt. Lett.* **38**, 609–611 (2013).
100. Plöschner, M., Tyc, T. & Čižmár, T. Seeing through chaos in multimode fibres. *Nat. Photon.* **9**, 529–535 (2015).
101. Weiss, U. & Katz, O. Two-photon lensless micro-endoscopy with in-situ wavefront correction. *Opt. Express* **26**, 28808–28817 (2018).
102. Choi, W. et al. Flexible-type ultrathin holographic endoscope for microscopic imaging of unstained biological tissues. *Nat. Commun.* **13**, 4469 (2022).
103. Gordon, G. S. D. et al. Characterizing optical fiber transmission matrices using metasurface reflector stacks for lensless imaging without distal access. *Phys. Rev. X* **9**, 041050 (2019).
104. Kuschmierz, R., Scharf, E., Koukourakis, N. & Czarske, J. W. Self-calibration of lensless holographic endoscope using programmable guide stars. *Opt. Lett.* **43**, 2997–3000 (2018).
105. Amitonova, L. V., Mosk, A. P. & Pinkse, P. W. H. Rotational memory effect of a multimode fiber. *Opt. Express* **23**, 20569–20575 (2015).
106. Li, S., Horsley, S. A. R., Tyc, T., Čižmár, T. & Phillips, D. B. Memory effect assisted imaging through multimode optical fibres. *Nat. Commun.* **12**, 3751 (2021).
107. Boonzajer Flaes, D. E. et al. Robustness of light-transport processes to bending deformations in graded-index multimode waveguides. *Phys. Rev. Lett.* **120**, 233901 (2018).
108. Tsvirkun, V. et al. Flexible lensless endoscope with a conformationally invariant multi-core fiber. *Optica* **6**, 1185–1189 (2019).
109. Stasio, N., Moser, C. & Psaltis, D. Calibration-free imaging through a multicore fiber using speckle scanning microscopy. *Opt. Lett.* **41**, 3078–3081 (2016).
110. Barankov, R. & Mertz, J. High-throughput imaging of self-luminous objects through a single optical fibre. *Nat. Commun.* **5**, 5581 (2014).
111. Rahmani, B., Loterie, D., Konstantinou, G., Psaltis, D. & Moser, C. Multimode optical fiber transmission with a deep learning network. *Light. Sci. Appl.* **7**, 69 (2018).
112. Kim, M. et al. Label-free neuroimaging in vivo using synchronous angular scanning microscopy with single-scattering accumulation algorithm. *Nat. Commun.* **10**, 3152 (2019).
113. Judkewitz, B., Horstmeyer, R., Vellekoop, I., Papadopoulos, I. N. & Yang, C. Translation correlations in anisotropically scattering media. *Nat. Phys.* **11**, 684–689 (2015).
114. Faccio, D., Velten, A. & Wetzstein, G. Non-line-of-sight imaging. *Nat. Rev. Phys.* **2**, 318–327 (2020).
115. Schott, S., Bertolotti, J., Léger, J.-F., Bourdieu, L. & Gigan, S. Characterization of the angular memory effect of scattered light in biological tissues. *Opt. Express* **23**, 13505–13516 (2015).
116. Kadobianskyi, M., Papadopoulos, I., Chaigne, T., Horstmeyer, R. & Judkewitz, B. Scattering correlations of time-gated light. *Optica* **5**, 389–394 (2018).
117. Osnabrugge, G., Horstmeyer, R., Papadopoulos, I., Judkewitz, B. & Vellekoop, I. Generalized optical memory effect. *Optica* **4**, 886–892 (2017).


## Acknowledgements

J.B. acknowledges funding from the Engineering and Physical Sciences Research Council (EPSRC) under grant number EP/T00097X/1. O.K. acknowledges funding from the European Research Council under the European Union's Horizon 2020 Research and Innovation Program grant number 101002406 and the Israel Science Foundation (grant number 1361/18).

## Competing interests

The authors declare no competing interests.

## Additional information

**Correspondence** should be addressed to Jacopo Bertolotti or Ori Katz.

**Peer review information** *Nature Physics* thanks Sébastien Popoff and the other, anonymous, reviewer(s) for their contribution to the peer review of this work.